Variability and long-term trends in the shelf circulation off eastern Tasmania

Eric C. J. Oliver[1,2] and Neil J. Holbrook[2,3]

Eric C. J. Oliver, eric.oliver@dal.ca

[1]Department of Oceanography, Dalhousie University, Halifax, Nova Scotia, Canada

[2]Institute for Marine and Antarctic Studies, University of Tasmania, Hobart, Tasmania, Australia

[3]Australian Research Council Centre of Excellence for Climate Extremes, University of Tasmania, Hobart, Tasmania, Australia

This article has been accepted for publication and undergone full peer review but has not been through the copyediting, typesetting, pagination and proofreading process, which may lead to differences between this version and the Version of Record. Please cite this article as doi: 10.1029/2018JC013994

Abstract. This study investigates trends and interannual variability of the marine climate across the continental shelf off eastern Tasmania for 1993–2016. This region is a hotspot for global warming and biodiversity. Eastern Tasmania lies at the boundary between two ocean currents (the East Australian Current Extension, or EAC Extension, and the Zeehan Current, ZC) leading to the local marine climate exhibiting trends and variability from both boundary currents. A numerical ocean model is used to provide high-resolution (∼2 km) estimates of the temperature, salinity and circulation for the region. Results indicate significant positive trends in temperature, salinity and southward flow over the shelf, consistent with an increasing EAC Extension. These trends are particularly strong in autumn, indicating a lengthening of the warm season. The interannual variability in the EAC Extension and ZC was quantified by a simple index, based on a modal analysis of surface circulation, indicating the relative dominance of each current. Strong EAC years were related to significantly more summertime marine heatwave days. Large-scale, remote drivers of variability were considered and we found weak but significant links with El Niño–Southern Oscillation (ENSO) and Tasman Sea Blocking (TSB). ENSO was found to modulate the EAC Extension in summer with a El Nio leading to enhanced southward flow and warming over the shelf. TSB was found to drive enhanced southward surface flow, particularly in winter. Nonetheless, large-scale forcing modes explain less than 25% of the total variability in the EAC-ZC system indicating that most of the variability is internally-generated.

Keypoints:

- Warming and salinification over the shelf is consistent with an enhanced East Australian Current (EAC) Extension
- The relative strengths of the EAC Extension and Zeehan Current relate significantly to marine heatwave occurrence
- El Niño–Southern Oscillation and the Tasman Sea Blocking are weakly related to interannual variations in circulation and temperature

1. Introduction

The near-surface waters off eastern Tasmania represent a global warming hotspot [*Holbrook and Bindoff*, 1997; *Ridgway*, 2007; *Hobday and Pecl*, 2014] and marine ecosystems there are under significant stress [*Ling*, 2008; *Johnson et al.*, 2011; *Oliver et al.*, 2017]. These waters form the southeastern portion of the 'Great Southern Reef' global biodiversity hotspot [*Bennett et al.*, 2016] and support large-scale fisheries and aquaculture industries [*Pecl et al.*, 2009; *Mayfield et al.*, 2012; *ABARE*, 2014]. The sensitivity of local ecosystems to both secular warming [*Johnson et al.*, 2011] and transient marine heatwave events [*Oliver et al.*, 2017, 2018] has been observed. However, the spatio-temporal patterns of historical temperature and salinity variability and trends at fine scales across Tasmania's eastern continental shelf and slope are less well-known. Constraining this past warming and variability will put ecological changes observed both in the nearshore and offshore zones east of Tasmania in context and better inform our expectations for future change under global anthropogenic warming.

Eastern Tasmania lies at the boundary between two ocean currents [*Wyrtki*, 1960; *Harris et al.*, 1987; *Cresswell*, 2000; *Ridgway*, 2007]. The East Australian Current (EAC) Extension, a southward extension of the South Pacific Gyre western boundary current, brings relatively warm and salty water south along Tasmania's east coast. The Zeehan Current (ZC) transports water southeastward along Tasmania's west coast and represents the final component in a series of boundary currents stretching back to the Leeuwin Current off Western Australia. The ZC opposes the EAC Extension to bring relatively cool and fresh water around the southern tip of Tasmania. This leads to the waters around

Tasmania being a mix, sourced from both the EAC Extension and the ZC, and subject to trends and variability from both boundary current systems. This system exhibits strong seasonal variability whereby in winter the ZC is dominant over the entire eastern Tasmanian continental shelf and in summer it retracts to the southern third of the shelf with the EAC Extension dominant over the northern two-thirds; autumn and spring are periods of transition between these two states during which the EAC Extension and ZC each extend over roughly half of the continental shelf's latitudinal range (e.g. *Oliver et al.* [2016]). Both long-term trends and variability in upper ocean temperatures have been noted to be large in this region [*Holbrook and Bindoff*, 1997; *Foster et al.*, 2014], with sea surface temperture warming at 3–4 times the global average rate. Long-term temperature and salinity trends are attributed to increased intensity of the southward penetration of the EAC Extension [*Ridgway*, 2007; *Sloyan and O'Kane*, 2015] which is expected to continue under anthropogenic climate change [*Oliver and Holbrook*, 2014].

This circulation also exhibits significant variability, which impacts the marine climate on the eastern Tasmanian continental shelf. Variability in the EAC Extension is dynamically linked on decadal time scales to large-scale wind forcing over the South Pacific [*Hill et al.*, 2008, 2011], which has been related to changes in the Southern Annular Mode or SAM [*Cai*, 2006; *Roemmich et al.*, 2007], and on seasonal-to-annual time scales to eddy-shedding events upstream [*Cetina-Heredia et al.*, 2014]. Additionally, on interannual time scales El Niño–Southern Oscillation (ENSO) has been shown to play a significant role in EAC separation and poleward transport along southeast Australia [*Cetina-Heredia et al.*, 2014], upper ocean temperature variations in the Tasman Sea [*Holbrook and Bindoff*, 1997; *Holbrook et al.*, 2005], subtropical mode water formation [*Sprintall et al.*, 1995;

Holbrook and Maharaj, 2008] and multi-year to decadal-scale changes in EAC transports [*Holbrook et al.*, 2011]. Tasman Sea Blocking (TSB) events also significantly affect the atmospheric circulation and rainfall patterns in the region [*Pook and Gibson*, 1999], and may influence the nearshore marine climate but this has yet to be demonstrated. Nearer to the Tasmanian coast, observations of trends and variability have been restricted to the relatively long Maria Island record which exhibits significant multi-decadal increases in temperature, salinity, and nitrate [*Kelly et al.*, 2015]. On the other hand, very little is known about the trends or variability in the ZC, or the spatial distribution of multi-decadal trends in temperature and salinity over the shelf.

A numerical ocean model, ETAS [*Oliver et al.*, 2016], is used here to provide high-resolution (∼2 km) estimates of the seawater temperatures, salinity and circulation over the eastern Tasmanian continental shelf. The mean state and seasonal cycle of circulation, temperature and salinity over the shelf has been described in *Oliver et al.* [2016]. Here we extend that study by performing a systematic analysis of multidecadal-scale trends and inter-annual variability off eastern Tasmania over the 24-year period from 1993 to 2016. We quantify the linear trends in surface and bottom temperature, salinity and currents over this period. We find a significant increase in EAC Extension penetration into the region with an associated increase in temperature and salinity throughout the water column, particularly in summer and autumn. The interannual variability of the circulation on the shelf is found to be dominated by the interplay of the EAC Extension and ZC, and an annual index is developed indicating the relative strength of these two currents over time. In both summer and winter we find that an anomalously strong EAC Extension (ZC) leads to an increased (decreased) probability of marine heatwave days. Finally, the

linear regression of temperature and circulation onto a set of climate modes indicates weak but statistically significant relationships with ENSO and TSB events. Perhaps somewhat surprisingly, no significant relationship was found with the mid- to high-latitude SAM. Overall, we found that much of the variance in our study region was unable to be explained by known large-scale climate modes, suggesting that a substantial fraction is internally generated.

2. Data and Methods

The data and methods are presented as follows: the high-resolution model data for temperature, salinity and circulation for the continental shelf off eastern Tasmania (Section 2.1), the calculation of linear trends both annual and seasonally (Section 2.2), the Empirical Orthogonal Function analysis technique for the decomposition of circulation and temperature into modes of variability (Section 2.3) and the regression method for calculating the role of climate modes of variability (Section 2.4).

2.1. ETAS ocean model

The Eastern TASmania (ETAS) coastal ocean model was used to provide daily records of three-dimensional ocean temperatures and currents off eastern Tasmania [*Oliver et al.*, 2016]. The model output covers the 24-year period from 1993 to 2016 and provides an unprecedented high-resolution estimate of the marine climate variations off eastern Tasmania. The ETAS model is an implementation of the Sparse Hydrodynamic Ocean Code [*Herzfeld*, 2006], a numerical ocean model designed to compensate for complex topography by using curvilinear grids. The ETAS model domain covers the eastern continental shelf of Tasmania from South Cape in the south to just north of Eddystone Point in

the northeast and offshore to just beyond the shelf break (∼2500 m depth, Figure 1a). The curvilinear model grid has a 200 x 120 grid cell configuration and an average horizontal resolution of ∼1.9 km (Figure 1b) with 43 vertical z-levels. National Centers for Environmental Prediction (NCEP) Climate Forecast System (CFS) Reanalysis (CFSR, 1993–2010, *Saha et al.*, 2010) and CFS Version 2 analysis (CSFv2, 2011–2016, *Saha et al.*, 2014) were used as boundary forcing at the surface, and Bluelink ReANalysis (BRAN, version 3, 1/1/1993–31/7/2012, *Oke et al.*, 2013) and OceanMAPS analysis (versions 2.0–3.1, 1/8/2012–31/12/2016; `wp.csiro.au/bluelink`) were used at the lateral boundaries. The model run used here includes freshwater runoff due to the two major rivers in the region (i.e. the Derwent and Huon Rivers), while tidal forcing was not included (i.e the R/NT run described by *Oliver et al.* [2016] with two additional simulation years: 2015–2016). Tidal forcing was neglected due to the difficulty in removing the tidal cycle from the daily snapshot output. The model provides daily, three-dimensional snapshots for the 1993-2016 period; data over the 1993–2014 period have been extensively validated against existing observations in the region [*Oliver et al.*, 2016]. Here, we have examined monthly- and seasonal-mean surface and bottom temperature, salinity, and circulation. In addition, daily surface temperatures were used to calculate marine heatwave days following the definition of *Hobday et al.* [2016].

The high-resolution simulation of the nearshore circulation, temperature and salinity from ETAS can be seen from four daily snapshots shown in Fig. 2. These snapshots also include the daily mean BRAN fields for comparison. The snapshot for 15 April 1993 (Fig. 2, first row) shows ETAS simulating sharp temperature and salinity fronts, particularly in the south of the domain, which are not evident on the same spatial scale in

BRAN. The snapshot for 15 Sept 2001 (Fig. 2, second row) shows how ETAS simulates a strong cross-shelf structure in the ZC as well as the influence on the circulation of the river runoff from the River Derwent and Huon River and the complex coastline around the Tasman Peninsula. The snapshot for 15 June 2003 (Fig. 2, third row) shows relatively uniform surface currents from BRAN while ETAS simulates a jet with strong cross-shelf structure (weakens closer to the coast) and strong salinity fronts near the coast in the northern portion of the domain. The snapshot for 15 April 2007 (Fig. 2, fourth row) shows how ETAS simulates a narrow filament of relatively cool water penetrating northeastwards from Tasman Peninsula as well as a narrow southward coastal current in the northern part of the domain. These snapshots provide evidence that the high spatial resolution of the ETAS model, including bathymetry and coastline, as well as the inclusion of river runoff allow it to simulate circulation, temperature and salinity features at a higher resolution than BRAN.

2.2. Annual and seasonal linear trends

Linear trends were calculated for surface and bottom temperature, salinity and currents by linear regression for both the monthly dataset and seasonal means, with regression coefficients estimated by ordinary least squares. The seasonal trends were calculated by first generating seasonal time series calculated by averaging the data over three-month blocks (summer: JFM, autumn: AMJ, winter: JAS, and spring: OND) and then using this time series for the linear regression. Statistical significances were obtained using a 95% confidence interval, and when zero fell outside this interval the trend was considered "statistically significant ($p < 0.05$)". Linear trends are expressed in units per decade. The linear regression was performed separately for u and v components of velocity and for

visualization the resulting trends are then plotted as a vector with the x and y components of the vector being the u and v trends respectively.

2.3. Empirical Orthogonal Function analysis

We perform an Empirical Orthogonal Function (EOF) analysis on monthly surface currents over the entire ETAS domain. Both East-West and North-South monthly surface velocities were combined into a single data matrix, on which the EOF analysis was performed. The time-mean was removed and each grid cell's data weighted by its cell area prior to the analysis. The weighting was performed to reduce the otherwise unrealistic weight given to the very many small grid cells in the estuaries, due to the curvilinear nature of the grid (Fig. 1b). The seasonal cycle was not removed prior to analysis. The inclusion of the seasonal cycle allows the first EOF to correspond to the seasonality which explains the largest proportion of the variance, namely the EAC Extension–ZC interplay (e.g. Fig. 1c; *Oliver et al.*, 2016). However, EOF1 also includes variability that does not strictly repeat each year from which we can extract the interannual variability of the EAC Extension–ZC confluence. Alternatively, we could have removed the seasonal cycle prior to performing the EOF analysis but there is no guarantee that the resulting mode would represent the EAC Extension–ZC system which is our focus and interest here.

The motivation of this analysis is to understand the role of circulation patterns in driving sea surface temperature variations and extremes. In particular, we wish to examine how variations in the dominant circulation features (i.e. the EAC Extension and the ZC) are expressed through sea surface temperature. Therefore, we first determine the temporal variability associated with these circulation features, via the EOF analysis described above, whereby the first mode represents variations in the EAC Extension and ZC system.

The associated patterns of sea surface temperature and marine heatwave days were then obtained by composite averaging those data based on years in which EOF1 was either anomalously positive or negative. The positive or negative states were determined from exceedances above or below the upper or lower tercile, respectively.

2.4. Climate modes and regression

We considered the influence of three modes of climate variability: El Niño–Southern Oscillation (ENSO), Southern Annular Mode (SAM), and Tasman Sea Blocking (TSB). Each mode was quantified using a monthly index. For ENSO we used the Multivariate ENSO Index (MEI; *Wolter and Timlin*, 1993, 1998)[1], for SAM we used the index of *Marshall* [2003][2], and for TSB we have the index of *Pook and Gibson* [1999] and *Marshall et al.* [2014], evaluated at 160°E (note: we also considered Tasman Sea Blocking at 140°E and the results were not strongly sensitive to this choice). The seasonal climatology and linear trend (over the analysis period: 1993–2016) were removed from each index prior to analysis.

The role of climate modes in modulating the marine climate was calculated by linear regression of monthly- and seasonal-mean surface and bottom temperature and currents onto each index independently, with regression coefficients estimated by ordinary least squares. Statistical significances were obtained using a 95% confidence interval, and when this interval did not include zero the relationship to the mode was considered "statistically significant ($p < 0.05$)". The linear regression was performed separately for u and v components of velocity and for visualization the resulting regression coefficients are then plotted as a vector with the x and y components of the vector being the regression coefficent for u and v respectively. Note that only zero-lag correlations were considered here.

3. Results

The results are presented as follows: the linear trends in surface and bottom properties (Section 3.1), the variability of the EAC Extension–ZC confluence region (Section 3.2), and the role of climate modes of variability (Section 3.3).

3.1. Long-term trends

Linear trends show warming and salinification of surface waters and an increase in southward surface flow along Tasmania's eastern shelf (Fig. 3a,b). At the bottom, linear trends show similar warming and salinification and increases in southward flow but this signal is restricted to over the shelf (here we define the shelf as being water depths $<$ 200 m; Fig. 3c,d). Off the shelf, we found northward trends in bottom flow and some weak cooling and freshening. These results indicate that over the shelf there is vertical coherency in the trends across all depths and variables while off the shelf we see a more baroclinic response with southward trends at the surface and northward trends at the bottom. It should also be noted that the trend in bottom temperature is greatest near the coast, decreasing towards the shelf edge. It should be noted that these trends are of a similar magnitude to the known biases whereby the model is up to 0.5°C warmer than remotely-sensed SST observations in the northern portion of the domain (Fig. 5c of *Oliver et al.* [2016]) and neglecting tides leads to a cool bias of $\sim$0.5°C to the east of the Tasman Peninsula (Fig. 12b of *Oliver et al.* [2016]).

Linear trends decomposed by season show surface warming evident in all seasons, but greatest in autumn (Fig. 4a–d, colours). Surface current trends indicate increasing southward flow for all seasons except winter, which exhibits a complex pattern with no general tendency (Fig. 4a–d, arrows). Bottom warming over the shelf shows less of a seasonal

variation but is nonetheless slightly higher in autumn (Fig. 4e–h, colours). Bottom current trends indicate increasing southward flows on the shelf and northward flows off the shelf, peaking in autumn and winter (Fig. 4e–h, arrows). The seasonal patterns of salinification are consistent with the warming patterns, except freshening is evident in Frederick Henry–Norfolk Bay (Fig. 5). It should be noted that the differences between seasonal trends are statistically significant only away from the coast, where the variation in the trend across the seasons is greatest.

3.2. Interannual variability

An EOF analysis of monthly surface currents was performed to decompose the variability into a set of circulation modes. Note that the seasonal cycle was not removed from the data prior to the EOF analysis being performed. EOF1 explains 47% of the total variance; while EOF2 explains only 13%. The spatial pattern of EOF1 is associated with alongshore flow over the entire domain (Fig. 6a). The maximum amplitude of EOF1 is in the central part of the domain, the region where the EAC Extension and ZC meet (Fig. 1c; *Oliver et al.*, 2016). The temporal variability of EOF1 was found by projecting the original data onto this mode (producing PC1; Fig. 7a, blue and red shading). The PC1 time series indicates a dominance of the seasonal cycle (Fig. 7a, grey line; estimated by harmonic regression onto the annual cycle and the first two harmonics). The seasonal timing of PC1 indicates southward flow (positive PC1) during summer and a northward flow (negative PC1) during winter, consistent with the seasonal cycle of the EAC Extension and ZC system (e.g. *Oliver et al.*, 2016). Therefore, we may interpret this mode as expressing the relative dominance of these two currents over the domain.

We note that the time series PC1 also exhibits significant non-seasonal variability (PC1-NS, defined by subtracting the seasonal cycle from PC1; Fig. 7b). In fact PC1-NS explains more than half (54%) of the total variance of PC1. The timing of positive and negative periods in PC1-NS indicate periods when the EAC Extension or ZC are anomalously strong or weak, relative to the expected seasonal variation. For example, the anomalously strong EAC extension in the summer of 2015/16 documented by *Oliver et al.* [2017] is evident as a period of positive PC1-NS at that time.

It may be helpful to distinguish between periods of positive or negative PC1-NS by the season in which they occur. Since the mean state varies significantly by season our interpretation of the impact of anomalous PC1-NS on the total flow will also differ by season. This was quantified by mapping the mean currents for summer and winter and adding to both the pattern associated with a ± 1 PC1-NS (Fig. 6b–e). The southward flow in the EAC Extension is dominant in summer and so a positive PC1-NS can be interpreted as an anomalously strong EAC Extension (Fig. 6b), while a negative PC1-NS can be interpreted as a weak EAC Extension with some ZC influence over the southern half of the domain (Fig. 6c). The ZC is dominant in winter and so a positive PC1-NS can be interpreted as a weak ZC with some EAC influence over the northern two-thirds of the domain (Fig. 6d), while a negative PC1-NS can be interpreted as an anomalously strong ZC (Fig. 6e).

The time variability of PC1-NS by season has been quantified in the annual time series by calculating the summer (JFM) and winter (JAS) mean PC1-NS, denoted PC1-NS-SUM and PC1-NS-WIN respectively (Fig. 7c,d). There is significant interannual variability in both seasons. The summer of 2016 shows the strongest EAC Extension signal on record

coinciding with the unprecedentend 2015/16 marine heatwave (MHW) event as described by *Oliver et al.* [2017]. The years with large-magnitude values of PC1-NS are indicated in red (positive) and blue (negative) in Fig. 7c,d, defined by exceedances above the upper tercile or below the lower tercile. This definition is used to define PC1-NS-SUM (+/-) and PC1-NS-WIN (+/-) years, below. The PC1-NS-SUM and PC1-NS-WIN time series are uncorrelated ($r = 0.01$, $p = 0.95$; non-zero lags were also considered) indicating that there is no persistence from one season to the next of the relative strength of the two currents; in other words, the state of the EAC Extension–ZC relationship from one season to the next is effectively independent. We can treat PC1-NS-SUM and PC1-NS-WIN as seasonal indices for the state of the EAC Extension–ZC system relative to the seasonal mean.

Composites of seasonal-mean SST anomalies with the PC1-NS-SUM and PC1-NS-WIN indices are larger in magnitude during the summer than during the winter (Fig. 8). In summer, PC1-NS-SUM is associated with relatively uniform shelf-wide anomalies of $\sim$1°C; positive for PC1-NS-SUM (+) years (strong EAC Extension; Fig. 8a) and negative for PC1-NS-SUM (-) years (weak EAC Extension; Fig. 8b). In winter, PC1-NS-WIN is associated with weaker anomalies, typically around $\pm$0.25°C, but distributed in a dipole pattern rather than uniformly across the shelf. A PC1-NS-WIN (+) (weak ZC; Fig. 8c) warms the shelf waters north and east of the Tasman Peninsula (climatologically EAC-influenced waters) and weakly cools (or has little effect on) the waters across the rest of the shelf to the south and west. A PC1-NS-WIN (-) (strong ZC; Fig. 8c) represents the opposite pattern with cooling over the region north and east of the Tasman Peninsula and weak warming elsewhere.

The impact of the EAC Extension–ZC state on SSTs in turn modifies the likelihoods of extreme SSTs, e.g. marine heatwaves (MHWs). Climatologically there are typically between 5 and 12 MHW days on average each summer, fewer near the coast and more offshore and over the southern portion of the domain (Fig. 9a). Composite averages of MHW days by phase of PC1-NS-SUM indicate that during PC1-NS-SUM (+) the count of summer MHW days is effectively doubled: 5–16 days along coastal regions and up to 28 days offshore particularly in the southern part of the domain (Fig. 9b). On the other hand, during PC1-NS-SUM (-) periods, total numbers of MHW days are suppressed so as to be essentially zero across the domain (Fig. 9c, note that we are using a lower limit of 5 days as per *Hobday et al.*, 2016). In the winter, climatologically there are between 5 and 9 MHW days per season (Fig. 9d). During PC1-NS-WIN (+) periods that number is effectively doubled across the domain (7–22 MHW days; Fig. 9e) while during PC1-NS-WIN (-) periods there is a near-total suppression of MHW days (Fig. 9f).

3.3. Large-scale climate drivers

The role of climate modes as remote drivers of the circulation was estimated by linear regression of known climate mode indices onto monthly- and seasonal-mean surface and bottom temperatures and currents, for winter and summer separately (Figs. 10 and Fig. 11). During summer, the MEI was found to be positively, and statistically significantly, correlated with warmer than average surface waters over most of the shelf and southward or southwestward surface flow over the southern third of the shelf (the ZC-dominated region; Fig. 10a). There was very little evidence of statistically significant correlations between the MEI and bottom temperature or currents, with only a small region of cooling and southwestward flow south of the Tasman Peninsula (Fig. 10d). During

winter, the MEI was signifcantly and negatively correlated with surface and bottom temperatures over the shelf portion of the ZC region in the South (Fig. 11a,d).

SAM did not generally have a strong relationship with temperatures or circulation. Specifically, SAM was not significantly correlated to temperatures except for small regions of negative correlations at the bottom in summer (Fig. 10e) and at both the bottom and surface in the ZC region in winter (Fig. 11b,e). SAM was significantly correlated with southwestward surface and bottom currents in winter in the ZC region (Fig. 11b,e), indicating that a positive SAM acts against the mean ZC flow.

TSB was most strongly related to surface flows. In summer, TSB was correlated with southward surface flow over the northern third of the domain, with associated coastal cooling at the surface, and southwestward surface flow over the southern third of the domain, with associated surface warming (Fig. 10c). At the bottom, TSB was not strongly correlated with flows but was negatively correlated with a broad region of bottom temperature in the southern portion of the domain (Fig. 10f). In winter, TSB was strongly correlated with the alongshore flow in the southward and southwestward direction but this relationship quickly decayed with depth leading to almost no relationship with bottom currents (Fig. 11c,f). TSB was not significantly correlated to winter temperatures at the surface or at the bottom.

Finally we tested if variability in the EAC Extension-ZC system, as characterised by PC1-NS, was related to these same large-scale climate modes. This was done by correlating PC1-NS with the modes using both the monthly time series (all months, summer-only, and winter-only) and the seasonal-mean time series (all months, summer-only i.e. PC1-NS-SUM, and winter-only i.e. PC1-NS-WIN; Table 1). Using the monthly data, we

found that PC1-NS is significantly ($p \leq 0.05$) correlated with the MEI for all months ($r = 0.20$) and particularly so for summer months ($r = 0.33$ for summer, not significant for winter). Tasman Sea Blocking was even more strongly related being statistically significant for all cases, with highest values in winter ($r = 0.42$). SAM was not significantly correlated with PC1-NS in any season. Using the seasonal-mean time series the only significant relationship found was with the MEI during summer, with a slightly higher value ($r = 0.45$) than that found using the monthly time series. Nonetheless, the variance explained by these modes combined is at most 26% (summing the monthly PC1-NS results for summer, noting that r^2 is variance explained and assuming the MEI and TSB explain independent proportions of the variance) leaving at least 74% of the variance unexplained.

4. Discussion and Conclusions

We have performed an analysis of decadal-to-multidecadal trends and interannual variability in a regional model of the marine climate in waters across the continental shelf off eastern Tasmania. Our results indicate strong positive trends in temperature, salinity and southward flow. Over the shelf, we found a coherent long-term trend of increasing southward flow, warming, and salinification extending over all depths. The co-variation of these three factors is consistent with the influence of a southward shift in the EAC [*Ridgway*, 2007], expressed as an intensification of the EAC Extension. On the other hand, off the shelf there was a more baroclinic response with increases in the southward flow and warming near the surface and increases in the northward flow and slight cooling at the bottom. The trends in warming were strongest in autumn indicating a lengthening of the warm season, and delaying the onset of the cool season. However, it should be noted that the model shows a seasonal SST peak ~10 days earlier than remotely-sensed observations and

propagates from the coast to offshore in opposition to the observed propagation [*Oliver et al.*, 2016] which presumably leads to a small cold bias in the mean during autumn. The warming trends at the bottom were much higher near the coast indicating that benthic ecosystems sensitive to warming may be more at risk in shallower, coastal waters than out on the shelf, further from shore. Care should to be taken not to over-interpret spatial patterns as the model exhibits biases in spatial structure in the mean and seasonal cycle of SST. Nonetheless, the general structure of the EAC Extension and ZC is well-reproduced by the model.

The interannual variability in the boundary current system off eastern Tasmania, the EAC Extension and ZC, was quantified by EOF analysis. Specifically, we developed an index for the state of the EAC-ZC system that quantifies the relative dominance of each current, seasonally. We found significant interannual variability in the EAC-ZC system with strong (weak) EAC years in summer leading to a doubling (complete offset) of marine heatwave days. Notably, a number of years with a strong EAC (in summer) or weak ZC (in winter) match well with known ecological impacts due to historical marine heatwaves, including kelp die-back in 2001 [*Valentine and Johnson*, 2004], mass abalone deaths in 2010 (Craig Mundy, IMAS, pers. comm.), aquacultured Atlantic salmon deaths in 2012 (Alistair Hobday, CSIRO, pers. comm.; *Hodgkinson et al.*, 2014), and a wide range of impacts from the extreme MHW in 2016 [*Oliver et al.*, 2017].

Modes of large-scale climate variability were examined for their role in driving marine climate variations off eastern Tasmania. We found that the strongest relationship was with El Niño–Southern Oscillation (ENSO) during summer whereby El Niño conditions were significantly correlated with warmer than average surface waters over most of the shelf and

anomalous southward or southwestward surface flow, consistent with an enhanced EAC Extension and previous findings of *Holbrook and Bindoff* [1997], *Holbrook et al.* [2011] and *Cetina-Heredia et al.* [2014]. Generally, El Niño seemed to drive circulation against the background ZC in the south for all seasons, and for both surface and bottom waters, while the effect in this region on temperature is less clear (excluding at the surface and in summer), with bottom waters cooling in summer and both surface and bottom waters cooling in winter. The Southern Annular Mode (SAM) had the weakest relationship with variability across the shelf but generally was found to act against the mean ZC flow in the southern portion of the domain. We speculate that the perceived inconsistency of our results with *Cai* [2006] and *Roemmich et al.* [2007], who find an important role for SAM in this region, may be due to the relatively short (interannual) time scale of response examined in this study compared with the long (decadal+) time scale examined in those studies. Tasman Sea Blocking was most strongly related to surface flows, driving southward currents particularly in winter, but was not significantly correlated to temperatures at the surface or at the bottom. This decoupling of surface circulation and SST in winter is consistent with results presented by *Oliver et al.* [2018] who found no surface circulation pattern to be associated with wintertime surface MHWs, indicating that wintertime SSTs may not be strongly controlled by surface currents.

We further compared these modes of variability against our index for variability in the EAC-ZC system. We found that El Niño was weakly, but nevertheless significantly, related to an enhanced EAC Extension in summer – consistent with *Cetina-Heredia et al.* [2014] who found ENSO explains about 10% of the variability of EAC transport. Tasman Sea Blocking was also found to be linked with modulating the EAC-ZC state, particularly

in winter. Despite these links, these modes leave a significant proportion of unexplained variance in the EAC-ZC system – at least 74%. This indicates that a large fraction of the interannual variance of the EAC-ZC system is not controlled by known large-scale climate modes, at least the ones we considered, and instead may be due to the interacting and cascading effects of shorter time-scale instabilities generated from local forcing [*Bull et al.*, 2017] and remotely forced contributions (e.g. *Holbrook et al.*, 2011, *Sloyan and O'Kane*, 2015) on time scales that are not accounted for by these large-scale modes.

Acknowledgments. ECJO was supported by funding from the Australian Research Council Centre (ARC) of Excellence for Climate System Science (ARCCSS; grant no. CE110001028). NJH acknowledges funding from the ARC Centre of Excellence for Climate Extremes (CLEX; Grant No. CE170100023). This paper makes a contribution to NESP Earth Systems Science and Climate Change Hub Project 2.3 (component 2) on the predictability of ocean temperature extremes. The ETAS ocean model data are available through the IMAS data portal (data.imas.utas.edu.au). We would like to thank Andrew Marshall (Bureau of Meteorology) for providing the Tasman Sea Blocking index time series.

Notes

1. https://www.esrl.noaa.gov/psd/enso/mei/

2. http://www.nerc-bas.ac.uk/icd/gjma/sam.html

References

ABARE (2014), *Australian fisheries and aquaculture statistics 2013, Research by the Australian Bureau of Agricultural and Resource Economics and Sciences*, Commonwealth of Australia.

Bennett, S., T. Wernberg, S. D. Connell, A. J. Hobday, C. R. Johnson, and E. S. Poloczanska (2016), The 'Great Southern Reef': social, ecological and economic value of Australia's neglected kelp forests, *Marine and Freshwater Research*, *67*(1), 47–56.

Bull, C., A. E. Kiss, N. C. Jourdain, M. H. England, and E. van Sebille (2017), Wind Forced Variability in Eddy Formation, Eddy Shedding, and the Separation of the East Australian Current, *Journal of Geophysical Research*, *122*, 9980–9998.

Cai, W. (2006), Antarctic ozone depletion causes an intesification of the Southern Ocean supergyre circulation, *Geophysical Research Letters*, *33*(L03712).

Cetina-Heredia, P., M. Roughan, E. van Sebille, and M. A. Coleman (2014), Long-term trends in the East Australian Current separation latitude and eddy driven transport, *Journal of Geophysical Research: Oceans*, *119*(7), 4351–4366.

Cresswell, G. (2000), Currents of the continental shelf and upper slope of Tasmania, in *Papers and Proceedings of the Royal Society of Tasmania*, vol. 133, pp. 21–30.

Foster, S. D., D. A. Griffin, and P. K. Dunstan (2014), Twenty years of high-resolution sea surface temperature imagery around australia: Inter-annual and annual variability, *PLoS one*, *9*(7), e100,762.

Harris, G., C. Nilsson, L. Clementson, and D. Thomas (1987), The water masses of the east coast of Tasmania: seasonal and interannual variability and the influence on phytoplankton biomass and productivity, *Marine and Freshwater Research*, *38*(5), 569–

590.

Herzfeld, M. (2006), An alternative coordinate system for solving finite difference ocean models, *Ocean Modelling*, *14*(3), 174–196.

Hill, K., S. R. Rintoul, R. Coleman, and K. R. Ridgway (2008), Wind-forced low frequency variability of the East Australian Current, *Geophysical Research Letters*, *35*(L08602).

Hill, K., S. R. Rintoul, K. R. Ridgway, and P. R. Oke (2011), Decadal changes in the South Pacific western boundary current system revealed in observations and ocean state estimates, *Journal of Geophysical Research*, *116*(C01009).

Hobday, A. J., and G. T. Pecl (2014), Identification of global marine hotspots: sentinels for change and vanguards for adaptation action, *Reviews in Fish Biology and Fisheries*, *24*(2), 415–425.

Hobday, A. J., L. V. Alexander, S. E. Perkins, D. A. Smale, S. C. Straub, E. C. Oliver, J. A. Benthuysen, M. T. Burrows, M. G. Donat, M. Feng, et al. (2016), A hierarchical approach to defining marine heatwaves, *Progress in Oceanography*, *141*, 227–238.

Hodgkinson, J. H., A. J. Hobday, and E. A. Pinkard (2014), Climate adaptation in australias resource-extraction industries: ready or not?, *Regional Environmental Change*, *14*(4), 1663–1678.

Holbrook, N. J., and N. L. Bindoff (1997), Interannual and decadal temperature variability in the southwest Pacific Ocean between 1955 and 1988, *Journal of Climate*, *10*(5), 1035–1049.

Holbrook, N. J., and A. M. Maharaj (2008), Southwest Pacific subtropical mode water: A climatology, *Progress in Oceanography*, *77*(4), 298–315.

Holbrook, N. J., P. S. Chan, and S. A. Venegas (2005), Oscillatory and propagating modes of temperature variability at the 3–3.5-and 4–4.5-yr time scales in the upper southwest Pacific Ocean, *Journal of climate*, *18*(5), 719–736.

Holbrook, N. J., I. D. Goodwin, S. McGregor, E. Molina, and S. B. Power (2011), ENSO to multi-decadal time scale changes in East Australian Current transports and Fort Denison sea level: Oceanic Rossby waves as the connecting mechanism, *Deep Sea Research Part II: Topical Studies in Oceanography*, *58*(5), 547–558.

Johnson, C. R., S. C. Banks, N. S. Barrett, F. Cazassus, P. K. Dunstan, G. J. Edgar, S. D. Frusher, C. Gardner, M. Haddon, F. Helidoniotis, et al. (2011), Climate change cascades: shifts in oceanography, species' ranges and subtidal marine community dynamics in eastern Tasmania, *Journal of Experimental Marine Biology and Ecology*, *400*(1), 17–32.

Kelly, P., L. Clementson, and V. Lyne (2015), Decadal and seasonal changes in temperature, salinity, nitrate, and chlorophyll in inshore and offshore waters along southeast Australia, *Journal of Geophysical Research: Oceans*, *120*(6), 4226–4244.

Ling, S. (2008), Range expansion of a habitat-modifying species leads to loss of taxonomic diversity: a new and impoverished reef state, *Oecologia*, *156*(4), 883–894.

Marshall, A. G., D. Hudson, H. H. Hendon, M. J. Pook, O. Alves, and M. C. Wheeler (2014), Simulation and prediction of blocking in the Australian region and its influence on intra-seasonal rainfall in POAMA-2, *Climate Dynamics*, *42*(11-12), 3271–3288.

Marshall, G. J. (2003), Trends in the Southern Annular Mode from observations and reanalyses, *Journal of Climate*, *16*(24), 4134–4143.

Mayfield, S., C. Mundy, H. Gorfine, A. M. Hart, and D. Worthington (2012), Fifty years of sustained production from the Australian abalone fisheries, *Reviews in Fisheries Science*, *20*(4), 220–250.

Oke, P. R., P. Sakov, M. L. Cahill, J. R. Dunn, R. Fiedler, D. A. Griffin, J. V. Mansbridge, K. R. Ridgway, and A. Schiller (2013), Towards a dynamically balanced eddy-resolving ocean reanalysis: BRAN3, *Ocean Modelling*, *67*, 52–70.

Oliver, E. C. J., and N. J. Holbrook (2014), Extending our understanding of South Pacific gyre 'spin-up': Modeling the East Australian Current in a future climate, *Journal of Geophysical Research*, *119*, 2788–2805, doi:10.1002/2013JC009591.

Oliver, E. C. J., M. Herzfeld, and N. J. Holbrook (2016), Modelling the shelf circulation off eastern Tasmania, *Continental Shelf Research*, *130*, 14–33.

Oliver, E. C. J., J. A. Benthuysen, N. L. Bindoff, A. J. Hobday, N. J. Holbrook, C. N. Mundy, and S. E. Perkins-Kirkpatrick (2017), The unprecedented 2015/16 Tasman Sea marine heatwave, *Nature Communications*, *8*, 16,101.

Oliver, E. C. J., V. Lago, A. J. Hobday, N. J. Holbrook, S. D. Ling, and C. N. Mundy (2018), Marine heatwaves off eastern Tasmania: Trends, interannual variability, and predictability, *Progress in Oceanography*, *161*, 116–130.

Pecl, G. T., S. D. Frusher, C. Gardner, M. Haward, A. J. Hobday, S. Jennings, M. Nursey-Bray, A. E. Punt, H. Revill, and I. E. Van Putten (2009), *The east coast Tasmanian rock lobster fishery–vulnerability to climate change impacts and adaptation response options. Report to the Department of Climate Change, Canberra*, Commonwealth of Australia.

Pook, M. J., and T. Gibson (1999), Atmospheric blocking and storm tracks during SOP-1 of the FROST Project, *Australian Meteorological Magazine*, (June Special Edition),

51–60.

Ridgway, K. R. (2007), Long-term trend and decadal variability of the southward penetration of the East Australian Current, *Geophysical Research Letters*, *34*(13), L13,613.

Roemmich, D., J. Gilson, R. Davis, P. Sutton, S. Wijffels, and S. Riser (2007), Decadal spinup of the South Pacific subtropical gyre, *Journal of Physical Oceanography*, *37*, 162–173.

Saha, S., S. Moorthi, H.-L. Pan, X. Wu, J. Wang, S. Nadiga, P. Tripp, R. Kistler, J. Woollen, D. Behringer, et al. (2010), The NCEP climate forecast system reanalysis, *Bulletin of the American Meteorological Society*, *91*(8), 1015–1057.

Saha, S., S. Moorthi, X. Wu, J. Wang, S. Nadiga, P. Tripp, D. Behringer, Y.-T. Hou, H.-y. Chuang, M. Iredell, et al. (2014), The NCEP climate forecast system version 2, *Journal of Climate*, *27*(6), 2185–2208.

Sloyan, B. M., and T. J. O'Kane (2015), Drivers of decadal variability in the Tasman Sea, *Journal of Geophysical Research*, *120*(5), 3193–3210.

Sprintall, J., D. Roemmich, B. Stanton, and R. Bailey (1995), Regional climate variability and ocean heat transport in the southwest Pacific Ocean, *Journal of Geophysical Research*, *100*(C8), 15,865–15,871.

Valentine, J. P., and C. R. Johnson (2004), Establishment of the introduced kelp undaria pinnatifida following dieback of the native macroalga Phyllospora comosa in Tasmania, Australia, *Marine and Freshwater Research*, *55*(3), 223–230.

Wolter, K., and M. S. Timlin (1993), Monitoring ENSO in COADS with a seasonally adjusted principal component index, in *Proc. of the 17th Climate Diagnostics Workshop*, vol. 5257.

Wolter, K., and M. S. Timlin (1998), Measuring the strength of enso events: How does 1997/98 rank?, *Weather*, *53*(9), 315–324.

Wyrtki, K. (1960), The surface circulation in the Tasman and Coral Seas, Aust. CSIRO Div. Fish. Oceanogr. Tech. Pap. No. 8.

Table 1. Correlations between PC1-NS and known large-scale climate modes. A dash indicates the correlation coefficent is not statistically significant at the 5% level.

	Monthly PC1-NS			Seasonal-mean PC1-NS		
Mode (Index)	All months	summer	winter	All months	summer	winter
ENSO	0.20	0.33	-	-	0.45	-
SAM	-	-	-	-	-	-
TSB	0.30	0.39	0.42	-	-	-

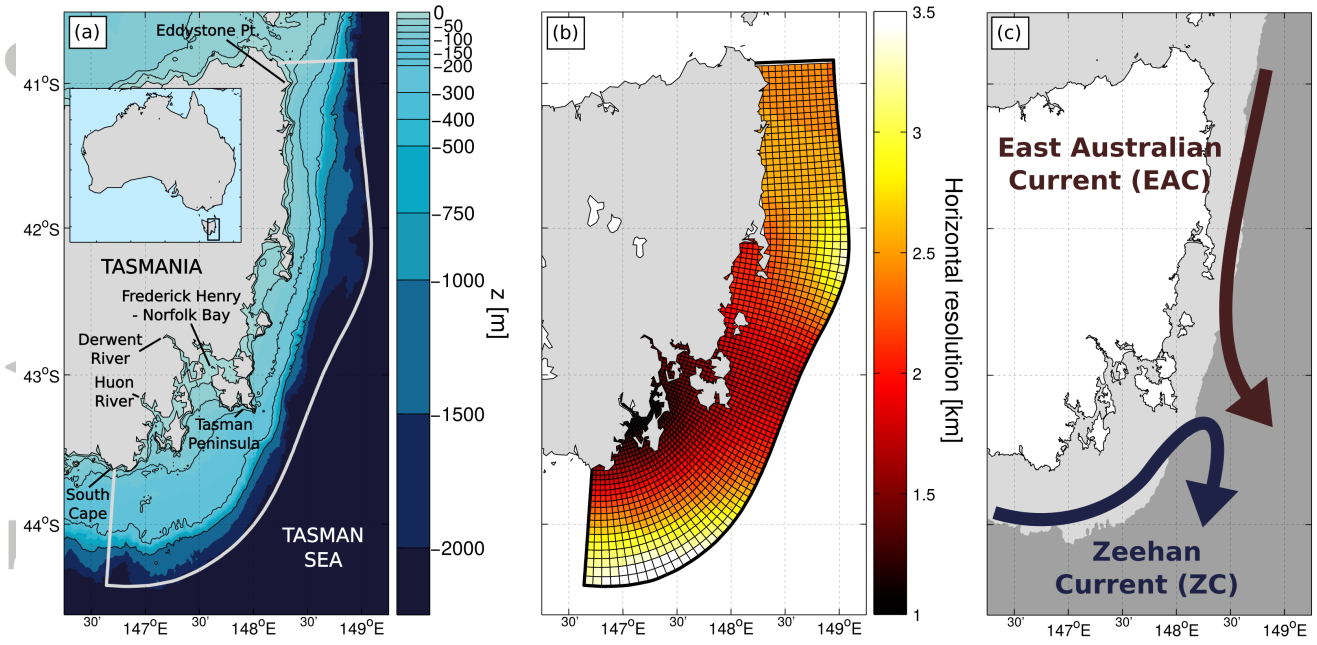

Figure 1. ETAS ocean model (a) model domain (white outline) and bathymetry (colors), (b) curvilinear grid and horizontal resolution, and (c) A schematic of the summer mean surface circulation with the Zeehan Current (ZC) and East Australian Current (EAC) Extension indicated. Adapted from Figure 1 in *Oliver et al.* [2018].

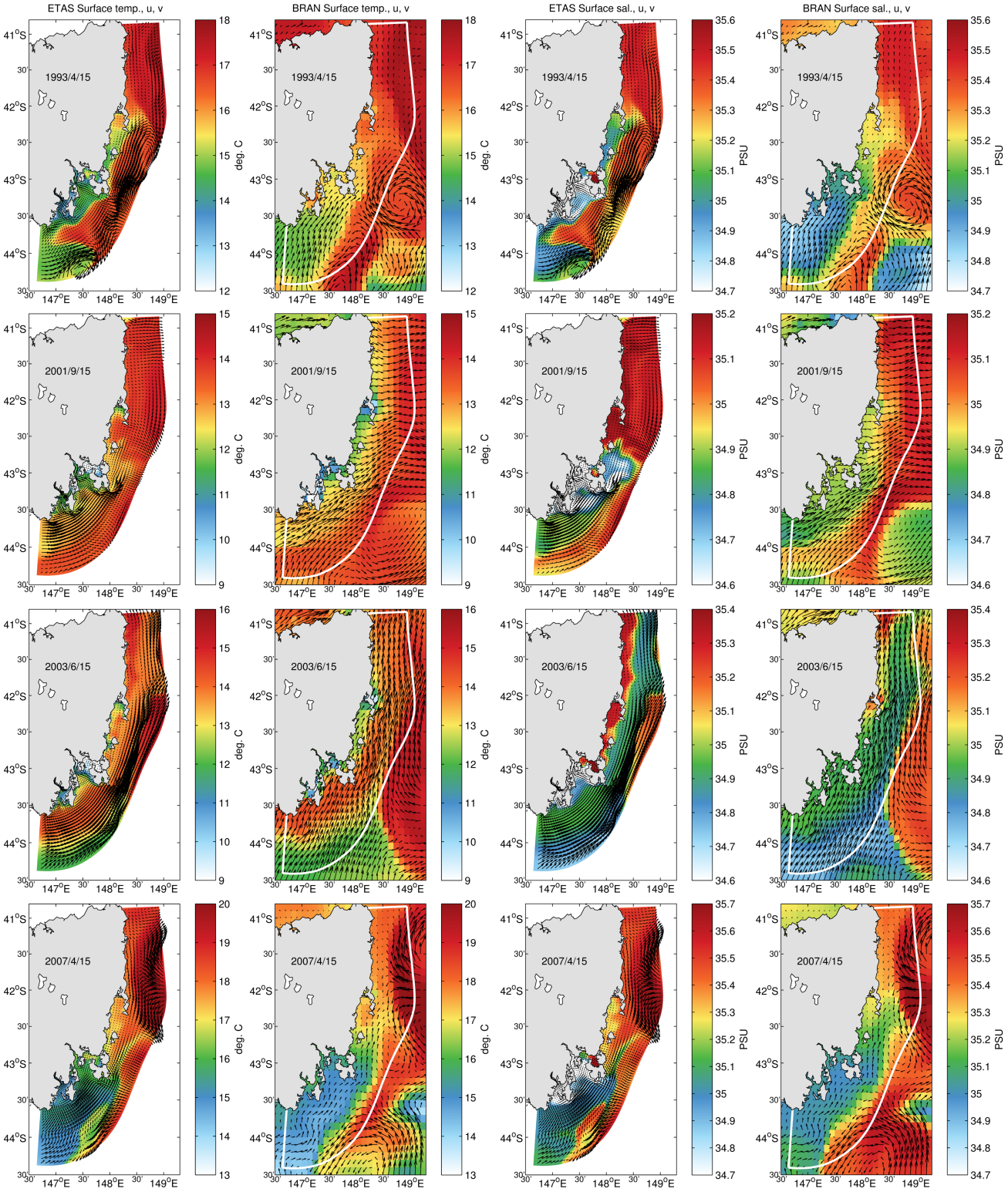

Figure 2. Daily snapshots from ETAS and BRAN output. Sea surface temperature, sea surface salinity and surface velocities are shown for ETAS and BRAN on (first row) 15 April 1993, (second row) 15 Sept 2001, (third row) 15 June 2003, and (fourth row) 15 April 2007.

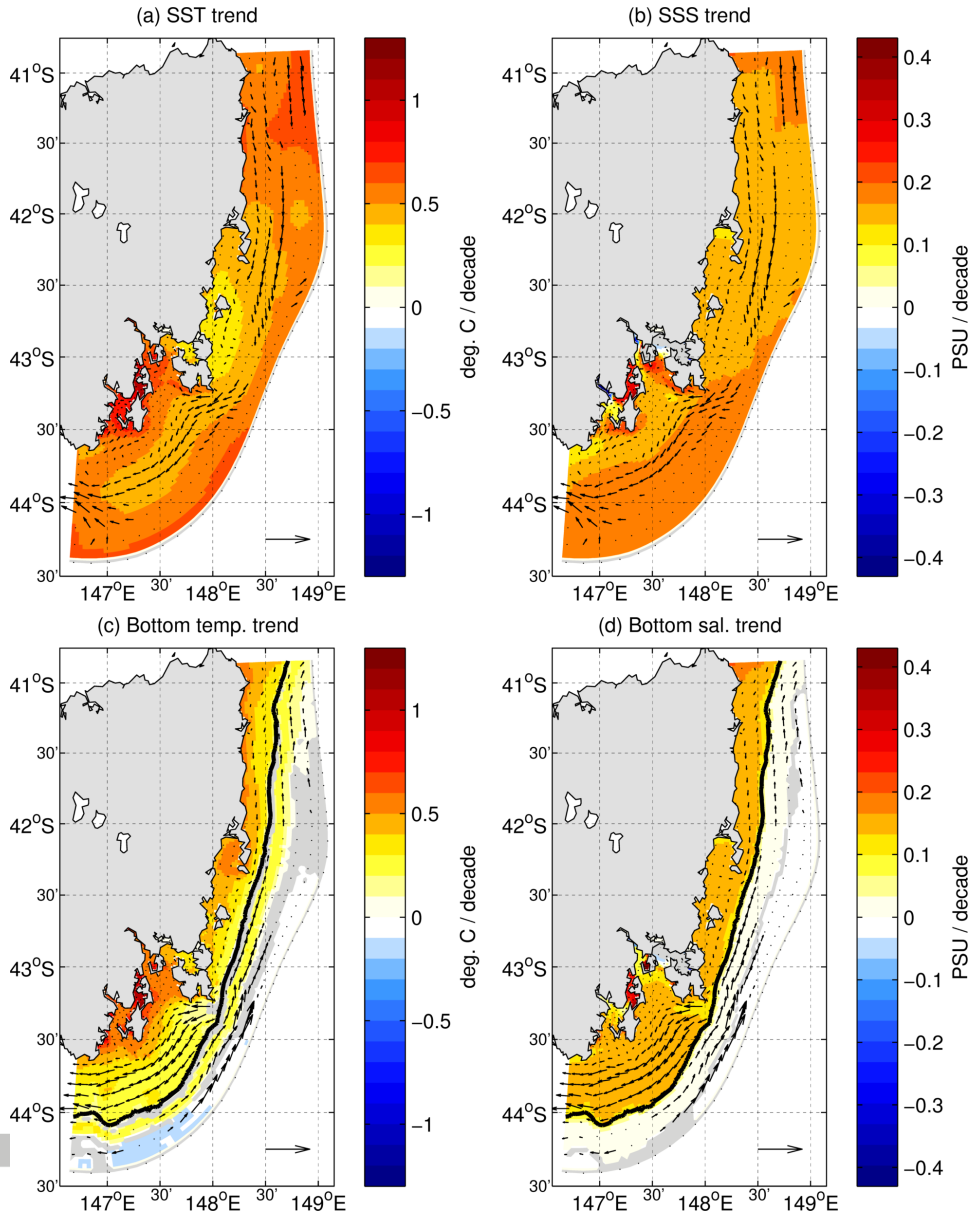

Figure 3. Linear trends in marine climate properties. Colours show linear trends (over 1993–2016) in temperature (left) and salinity (right) at the surface (top) and bottom (bottom), in units of °C decade^{-1} and PSU decade^{-1} respectively. Arrows show linear trends in surface and bottom currents, with the reference arrow in the bottom left of each panel indicating a trend of 0.1 m s^{-1} decade^{-1}. The solid black contour indicates the 200 m isobath. Grey indicates temperature or salinity trends that are not significantly different from zero at the 5% significance level; trends in velocities that were not significant at this level were not plotted.

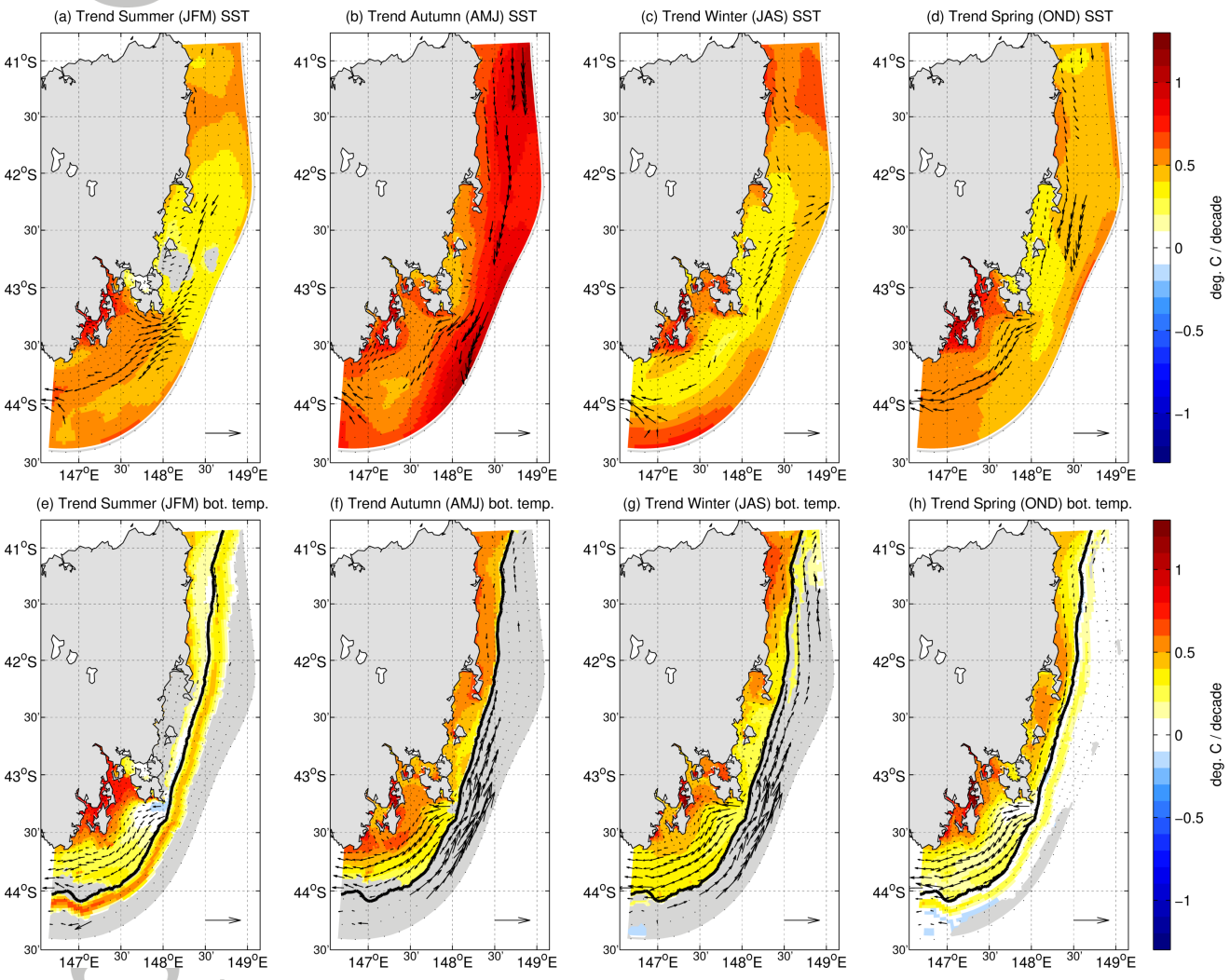

Figure 4. Linear trends in seawater temperature, by season. Trends of surface (top) and bottom (bottom) temperature are shown for (left–to–right) summer (JFM), autumn (AMJ), winter (JAS) and spring (OND). Otherwise format is the same as Fig. 3.

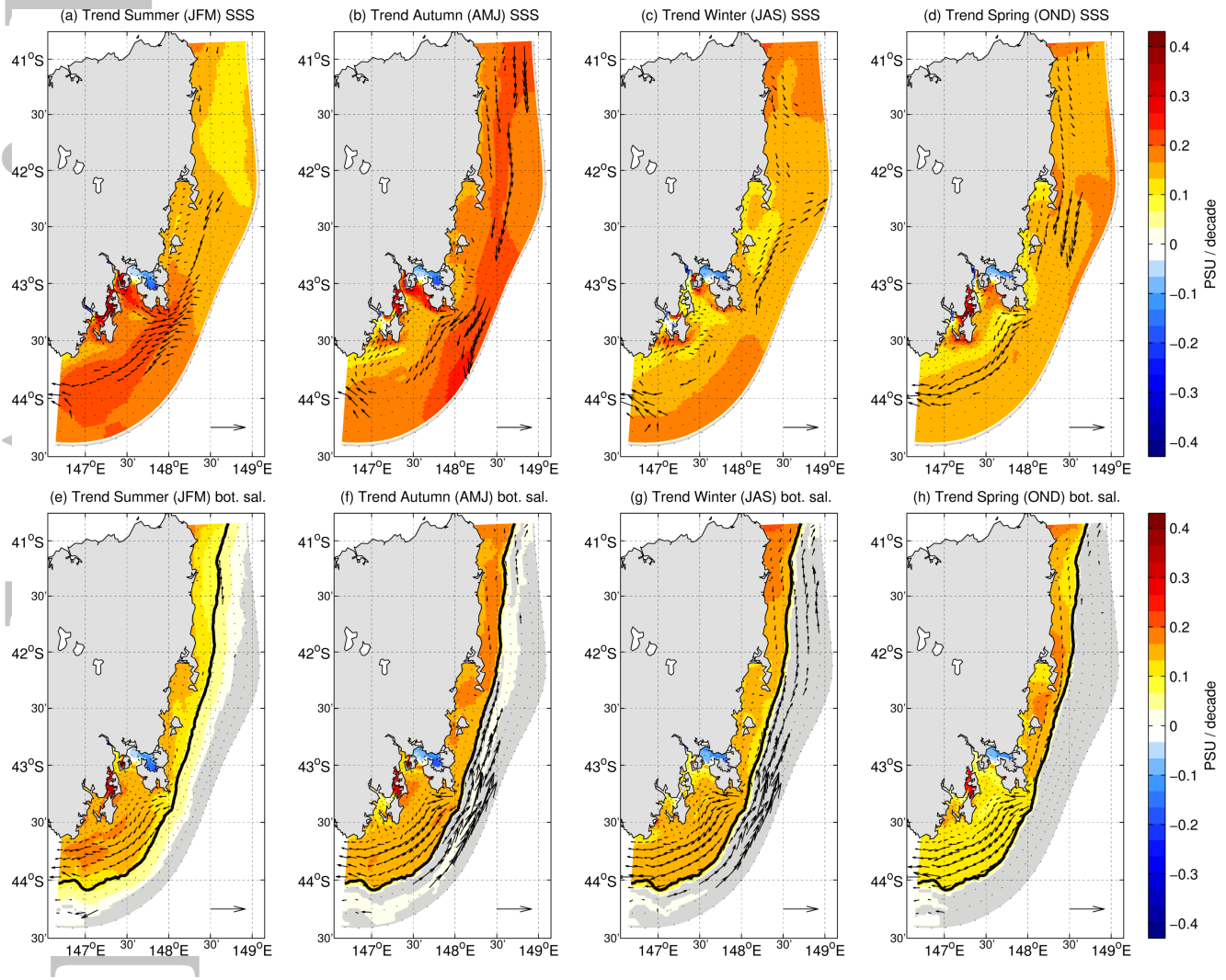

Figure 5. Linear trends in salinity, by season. Format is the same as Fig. 4.

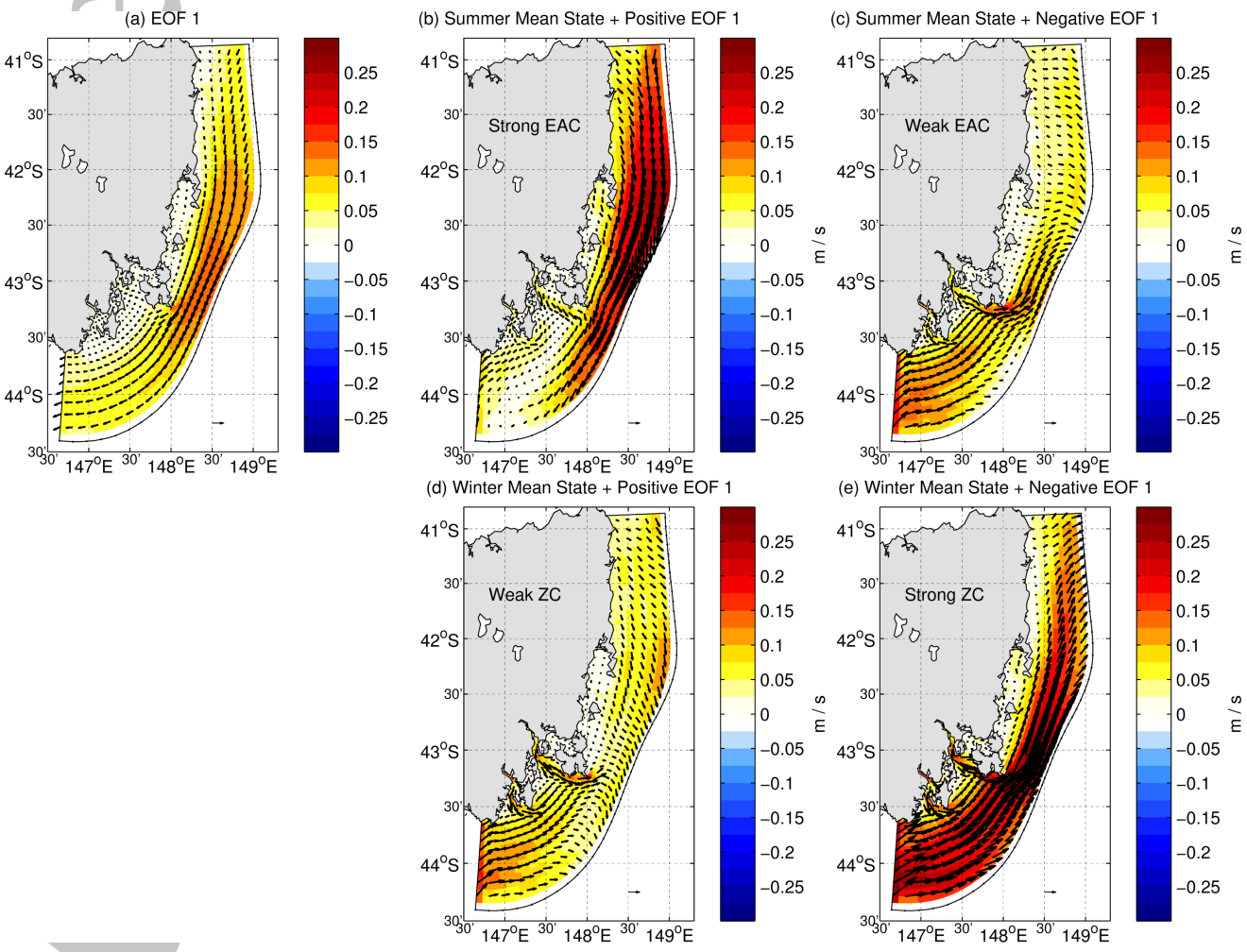

Figure 6. First Empirical Orthogonal Funtion (EOF1) of surface currents. (a) The spatial pattern associated with EOF1. This mode can occur in both summer and winter and panels (b–e) show the spatial pattern of (b,c) mean summer and (d,e) mean winter circulation superimposed with an anomalous (b,d) positive and (c,e) negative EOF1 state. Colours indicate current speeds and the reference arrow in the bottom right of each panel represents 0.1 m s^{-1}.

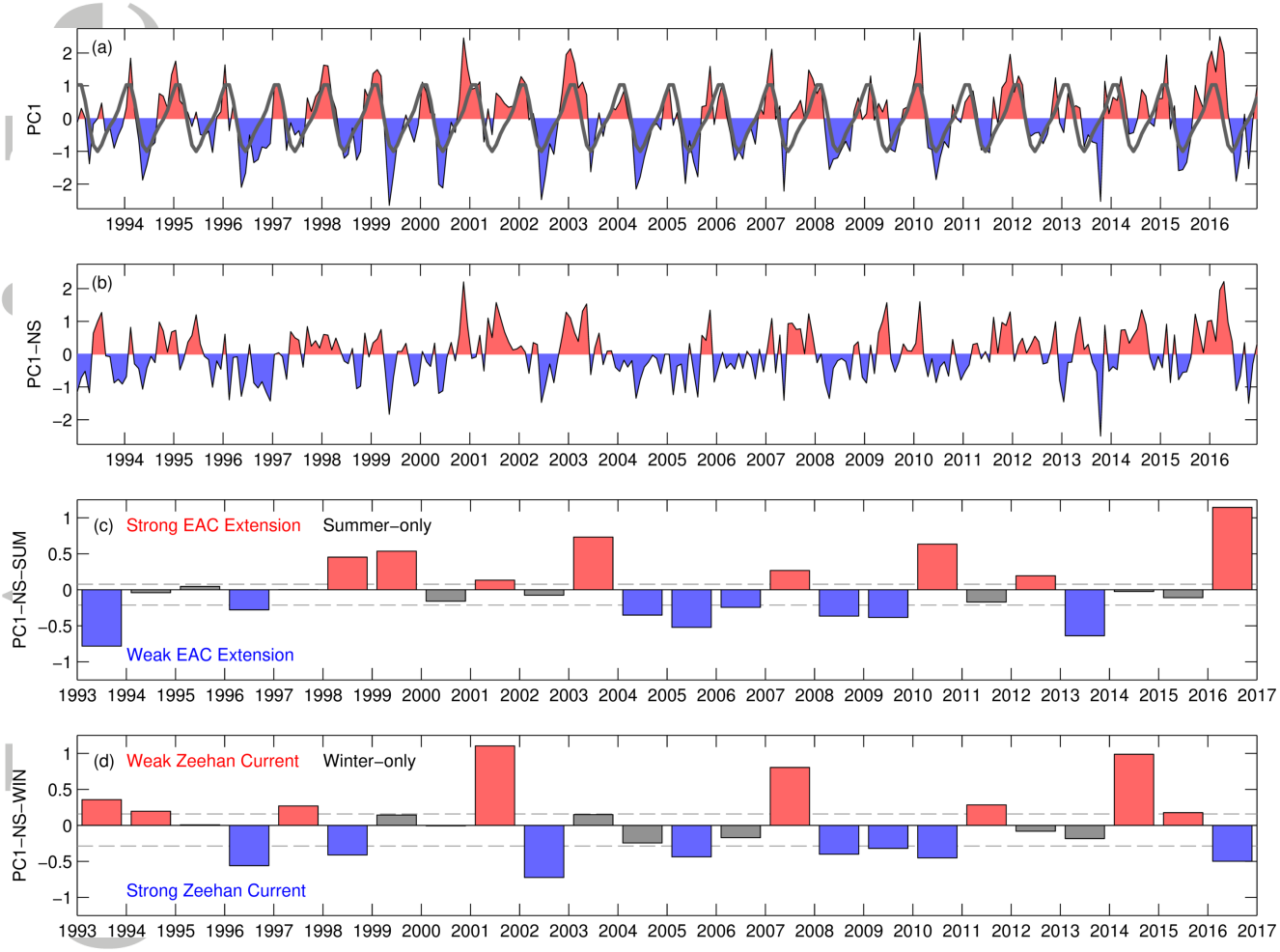

Figure 7. Principal Component time series (PC1) associated with EOF1. PC1 is shown in (a) as thin black line and red and blue shading along with its seasonal cycle (thick grey line). The anomalies of PC1 relative to the seasonal cycle, PC1-NS, is shown in (b). The seasonal mean time series' of PC1-NS are shown for (c) summer and (d) winter. Seasonal means that are larger than the upper tercile (positive dashed line) are shown as red, lower than the lower tercile (negative dashed line) are shown as blue, and all others are shown as grey.

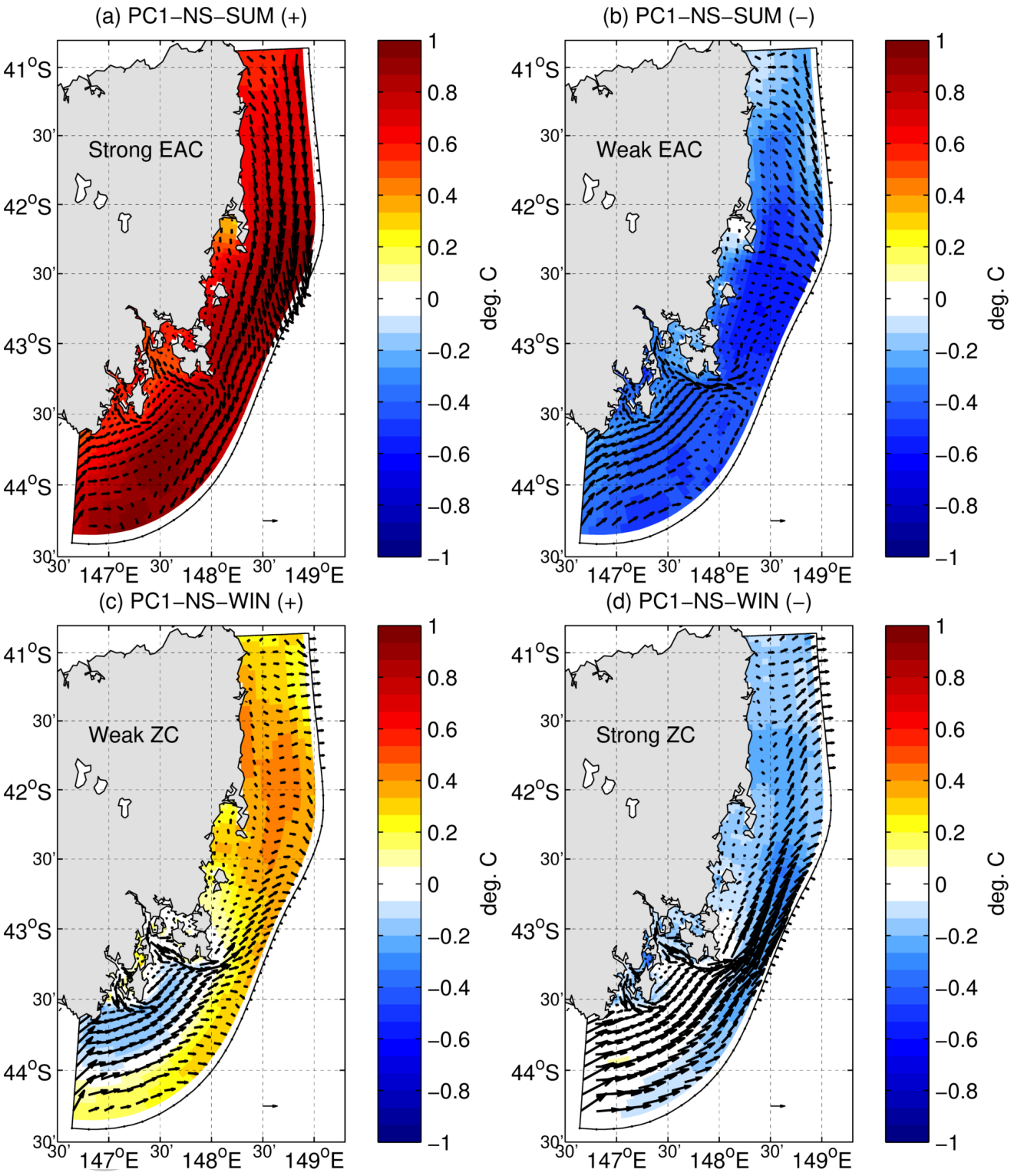

Figure 8. Response of SST to the EAC Extension–ZC system. Colours (arrows) indicate the composite mean SST (surface currents) seasonal anomalies for years with (a) PC1-NS-SUM (+), (b) PC1-NS-SUM (-), (c) PC1-NS-WIN (+) and (d) PC1-NS-WIN (-). The reference arrow in the bottom right of each panel represents 0.1 m s^{-1}.

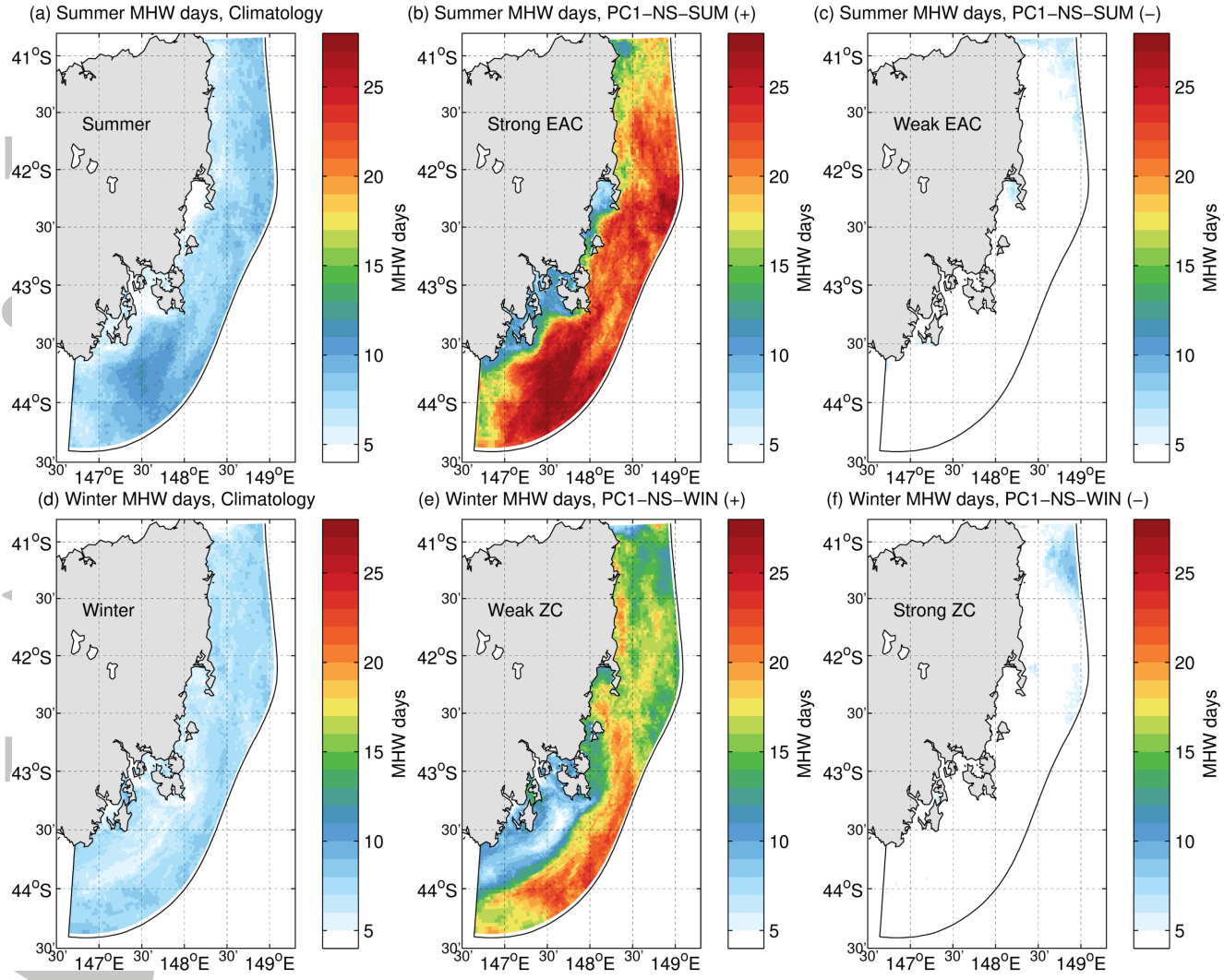

Figure 9. Response of MHW days to the EAC Extension–ZC system. The climatological mean count of MHW days across all years (1993–2016) is shown for (a) summer and (d) winter. The composite mean count of MHW days is shown for summer during (b) PC1-NS-SUM (+) and (c) PC1-NS-SUM (-) years and for winter during (e) PC1-NS-WIN (+) and (f) PC1-NS-WIN (-) years. Heatwave days fewer than 5, below the minimum duration threshold of *Hobday et al.* [2016], are shown in white.

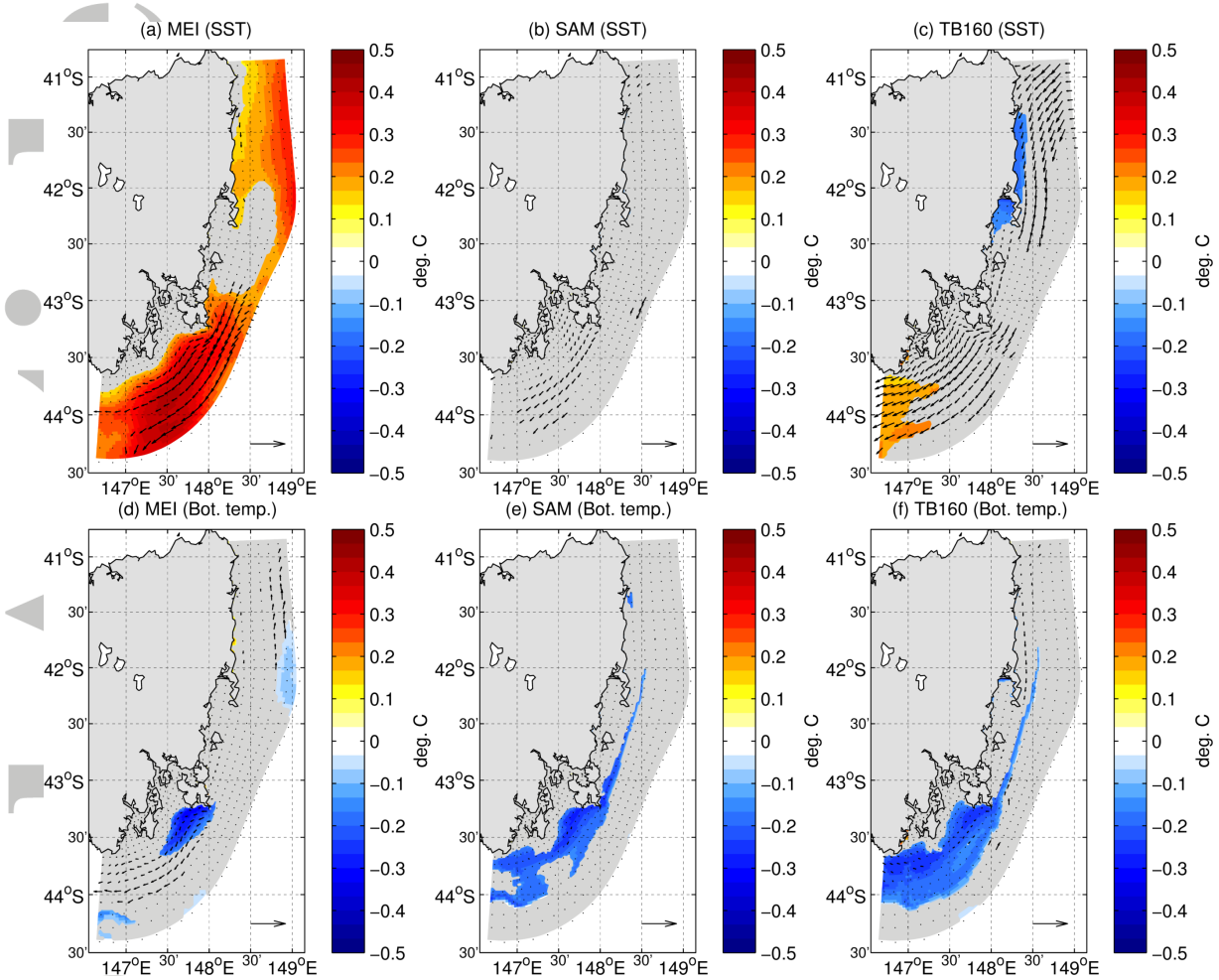

Figure 10. Relationship between known large-scale climate modes and marine climate, in summer. Colours indicate regression coefficients for (top) surface and (bottom) bottom temperature with the indices of (a,d) ENSO (represented by the MEI), (b,e) SAM, and (c,f) TSB. Arrows indicated regression coefficents for currents, the reference arrow in the bottom right of each panel represents 0.1 m s^{-1}. Grey indicates that the regression coefficients for temperature were not statistically significantly different from zero at the 5% significance level; regression coefficients for velocities that were not significant at this level were not plotted.

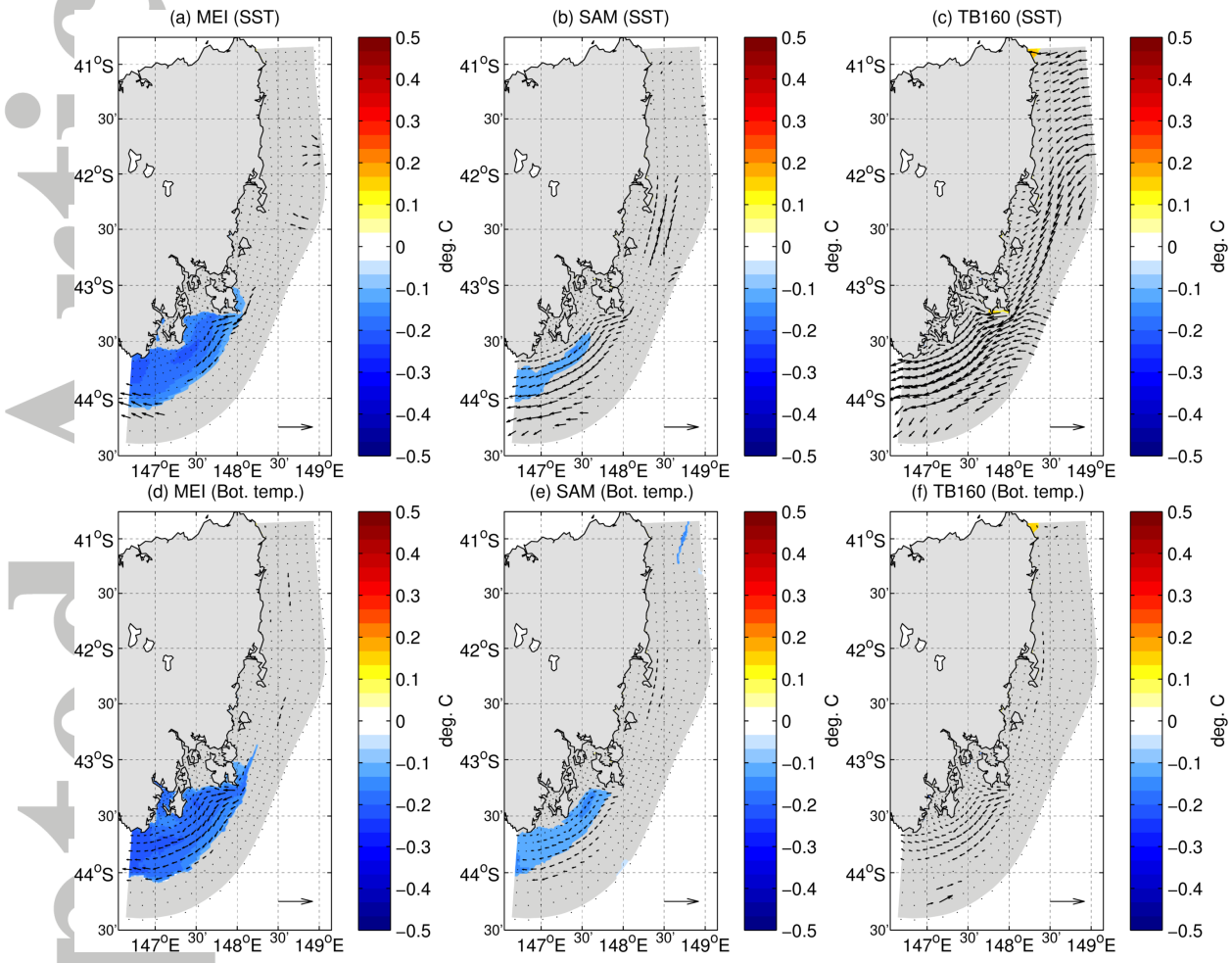

Figure 11. Relationship between known large-scale climate modes and marine climate, in winter. Format as in Fig. 10.